ACS OMEGA

http://pubs.acs.org/journal/acsodf

Article

Dodonaea angustifolia Extract-Assisted Green Synthesis of the Cu_2O/Al_2O_3 Nanocomposite for Adsorption of Cd(II) from Water

Yeshi Endris Hassen, Gangaraju Gedda, Ayalew H. Assen, Daniel Manaye Kabtamu, and Wubshet Mekonnen Girma*

Cite This: *ACS Omega* 2023, 8, 17209−17219

Read Online

ACCESS | Metrics & More | Article Recommendations

ABSTRACT: The enhanced worldwide concern for the protection and safety of the environment has made the scientific community focus their devotion on novel and highly effective approaches to heavy metals such as cadmium (Cd) pollutant removal. In this research, *Dodonaea angustifolia* plant extract-mediated Al_2O_3 and Cu_2O nanoparticle (NP) syntheses were accomplished using the coprecipitation method, and the Cu_2O/Al_2O_3 nanocomposite was prepared by simple mixing of Cu_2O and Al_2O_3 NPs for the removal of Cd(II) ions from aqueous solution. Therefore, an efficient green, economical, facile, and eco-friendly synthesis method was employed, which improved the aggregation of individual metal oxide NPs. The chemical and physical properties of the nanocomposite were examined by different characterization techniques, including scanning electron microscopy (SEM), X-ray diffraction (XRD), Fourier transform infrared spectroscopy (FT-IR), and Brunauer−Emmett−Teller (BET) surface area analysis. Furthermore, the performances of the nanoadsorbents for the adsorptive eradication of Cd^{2+} ions from water were investigated. The influence of pH, contact time, initial Cd quantity, and nanocomposite amount on adsorption effectiveness was carefully studied. The adsorption rates of the Cu_2O/Al_2O_3 nanocomposite were rapid, and adsorption equilibrium was attained within 60 min for 97.36% removal of Cd(II) from water. The adsorption isotherm data were best fitted by the pseudo-second-order kinetic and Langmuir isotherm models with the highest adsorption ability of 4.48 mg/g. Therefore, the synthesized Cu_2O/Al_2O_3 nanocomposite could be a potential candidate for a highly efficient adsorbent for heavy metal ion removal from aqueous solutions.

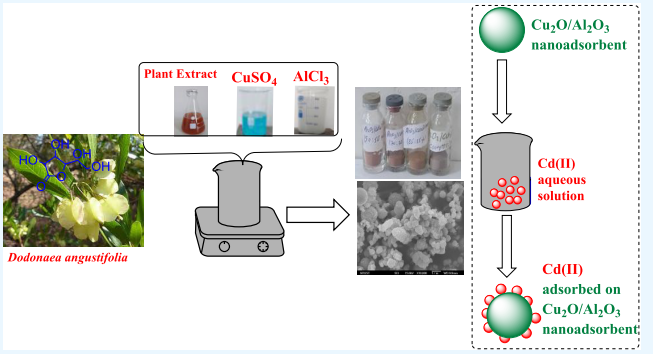

1. INTRODUCTION

Contamination of heavy metals, including cadmium (Cd), in water creates a serious hazard to living organisms, including human health, due to their toxicity, carcinogenicity, and non-biocompatibility.[1] They enter the living system via the food chain, eventually leading to numerous health disorders in humans. The sewage from battery manufacturing, metallurgical, and mining processes is the major origin of heavy metal contaminants. In order to safeguard the quality of drinking water and protect human health, it is crucial to eradicate heavy metals from polluted water.[2]

Traditional approaches such as reverse osmosis, ion exchange, electro-coagulation, ultrafiltration, filtration, micro-extraction, photocatalysis, chemical precipitation, membrane separation, electrolysis/electroplating, and adsorption have been developed for the amputation of contaminations from water.[3] However, the majority of these approaches have technical and economical limitations, including operational as well as high capital costs, more sensitivity toward operative conditions, a huge amount of sludge production, and substantial energy usage. Among these approaches, the adsorption strategy has universally been considered one of the generally used strategies for the removal of heavy metals because of its low operating cost, simple operation, and high accessibility.[4,5] Consequently, a variability of adsorbents including activated carbon/charcoal, zeolite, and bentonite was used for the effective removal of heavy metals.[4] But these traditional adsorbents typically show low adsorption ability and poor separation performance. As a result, there is a growing interest in developing novel adsorbents through chemical modification or combining them with various supporting materials.

Received: March 9, 2023
Accepted: April 24, 2023
Published: May 2, 2023

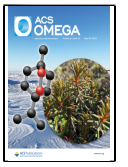

Recent advancement and invention of delightful NPs by nanoscience and technology help developments in environmental applications.[6,7] Specifically, the nanomaterial-integrated adsorption method is gaining significant attention for wastewater treatment to address the emerging issue of heavy metal pollution.[8] Therefore, various nanoadsorbents, including graphene,[9] carbon nanotubes,[10] metal and metal oxides,[11] nanocomposites,[12] etc., have been extensively explored as nanoadsorbents for the eradication of various heavy metal pollutants from wastewater. Among them, metal oxide nanomaterials such as Al_2O_3 and Cu_2O and their composite are recognized as remarkable materials due to their availability, tunable and plentiful surface-active sites, low toxicity, and economic viability.[13] These features make them significant materials for rapid, sensitive, and effective adsorptive removal of various heavy metal ions such as Cd^{2+}, Hg^{2+}, and Pb^{2+}. Besides this, researchers devoted their work to fabricate metal oxide-based hybrid nanocomposites by integrating two or more metal oxide nanomaterials to enhance the heavy metal removal absorption capacity.[14] Interestingly, the metal oxide nanocomposites avoided aggregation of materials and showed improved heavy metal adsorption performances.[7,15] In this line, various kinds of composites such as Fe_2O_3/Al_2O_3,[16] polythiophene/Al_2O_3,[17] polyaniline/Al_2O_3,[18] poly(vinylidene fluoride) (PVDF)/poly(vinyl alcohol) (PVA)/Al_2O_3,[19] Cu_2O/ZnO,[20] Fe_2O_3/Cu_2O,[21] and TANI/Cu_2O/Ag[22] have been reported for the removal of a variety of metal ions such as As(V), Pb(II), Zn(II), Cd(II), Cu(II), Pb(II), Ni(II), and Hg(II) ions. However, most of the composites' preparation is limited by either a complicated and time-consuming synthesis process or the usage of expensive/toxic chemicals. Hence, there is a dire need to develop novel, eco-friendly, facile, and green synthesis approaches for the production of metal oxide nanocomposite for effective heavy metal removal.

This work aims to develop a green, economical, facile, and eco-friendly synthesis method to prepare the Cu_2O/Al_2O_3 nanocomposite and explore its feasibility of removing Cd(II) from aqueous solutions. Herein, we used plant leaf (*Dodonaea angustifolia*) extract as a reducing and protecting agent for forming the Cu_2O/Al_2O_3 nanocomposite. After the successful synthesis of the target nanocomposites, various experiments were performed to test the effectiveness of the removal process. The effects of time, adsorbent amount, Cd(II) ion concentration, and solution pH on the eradication of Cd(II) ions were evaluated. Langmuir and Freundlich isotherms were verified to confirm adsorption processes. Kinetic studies were conducted to examine the influence of time on the Cd(II) removal process.

2. MATERIALS AND METHODS

2.1. Chemicals and Reagents. Aluminum chloride ($AlCl_3{\cdot}6H_2O$, 97%), copper(II) sulfate ($CuSO_4{\cdot}9H_2O$, 99%), cadmium nitrate ($Cd(NO_3)_2$, 99%), zinc nitrate ($Zn(NO_3)_2{\cdot}6H_2O$, 98%), magnesium nitrate hexahydrate ($Mg(NO_3)_2{\cdot}6H_2O$, 99%), nickel(II) nitrate hexahydrate ($Ni(NO_3)_2{\cdot}6H_2O$, 99%), lead nitrate hexahydrate ($Pb(NO_3)_2{\cdot}6H_2O$, 99%), calcium nitrate tetrahydrate ($Ca(NO_3)_2{\cdot}4H_2O$, 99%), sodium hydroxide (NaOH, 99.8%), ethanol (CH_3CH_2OH, 99.9%) were used. All reagents are analytical grade and used without any additional purification.

2.2. Preparation of *D. angustifolia* Plant Extract. Fresh, matured, and green *D. angustifolia* leaves were collected from Haiq, South Wollo, Ethiopia. The collected leaves were cleaned with tap water and distilled water to remove the layer of dust particles. The clean leaves were subjected to drying at room temperature in the absence of light. The dried plant leaves were then crushed and ground with an electrical grinder. The powder (50 g) was placed in an Erlenmeyer flask with 500 mL of distilled water and kept at 80 °C for 1 h under a magnetic stirrer. The attained result solution was permitted to cool at ambient temperature and filtered over Whitman no. 1 filter paper to obtain a clear solution. Finally, the obtained filtrate was kept at 4 °C for further use.

2.3. *D. angustifolia* Plant Extract-Mediated Synthesis of Cuprous Oxide (Cu_2O) NPs. The synthesis of Cu_2O was carried out by following literature procedures with some modifications.[23] In brief, *D. angustifolia* plant extract was used as the template/capping and reducing agent in an aqueous solution. $CuSO_4{\cdot}5H_2O$ was first dissolved in 100 mL of distilled water to produce a 0.1 M precursor salt solution. After that, 10 mL of an aqueous plant extract was added to a 0.1 M $CuSO_4{\cdot}5H_2O$ solution. Subsequently, the two solutions were mixed and stirred for 30 min at 70 °C in a hot plate with a magnetic stirrer, until the blue color altered to an everlasting reddish-brown suspension signifying the formation of Cu_2O NPs. The solution was cooled to room temperature, decanted, and cleaned many times using distilled water. The brick-red product was dried at 60 °C for 24 h in a hot air oven.

2.4. *D. angustifolia* Plant Extract-Mediated Synthesis of Al_2O_3 NPs. To 100 mL of a 0.1 M $AlCl_3{\cdot}6H_2O$ solution, 100 mL of *D. angustifolia* plant extract was added dropwise with stirring using a magnetic stirrer. Subsequently, NH_3 (0.1 M) was added until the pH reached 7, and then the solution was allowed to stir for 30 min at room temperature. The resultant solution was kept at room temperature for 1 day to permit the NPs to settle completely. After 24 h, it was centrifuged for 15 min at 12 000 rpm, and the extracted precipitate was washed three times with ethanol. Subsequently, it was dried at 80 °C for 12 h in a hot air oven, and then the white precipitate was calcined in a muffle furnace for 3 h at a temperature of 1000 °C.

2.5. *D. angustifolia* Plant Extract-Mediated Synthesis of Cu_2O/Al_2O_3 Nanocomposites. The plant extract-mediated Cu_2O/Al_2O_3 nanoadsorbent was synthesized with a simple physical approach. In this experiment, nanocomposites were prepared by combining different mass ratios of Cu_2O and Al_2O_3 NPs (Cu_2O/Al_2O_3: 50/50, 30/70, 15/85, and 5/95%). The components were thoroughly mixed using a mortar and pestle and subsequently calcined at 250 °C for 2 h.

2.6. Batch Adsorption Experiments. Batch adsorption tests were carried out to inspect the adsorption potentiality of Cu_2O/Al_2O_3 nanocomposites to remove Cd(II) from aqueous solution. To evaluate the adsorption feasibility of the nanocomposite, different experiments, such as pH, adsorbent mass, contact time, and initial Cd(II) quantity, were studied. About 0.1−0.4 g of the adsorbent (Cu_2O/Al_2O_3 nanocomposites) was added into an aqueous solution of cadmium, stirred for 4 h, left at 24 h till the equilibrium was attained, and then filtered through Whatman filter paper. The optimum amount of the nanoadsorbent was gained by plotting a graph between percentage removal and the adsorbent's mass. The effects of interaction time, Cd(II) ion quantity, and pH were studied in the ranges of 30−120 min, 30−120 mg/mL, and 2−10, respectively. The adsorption experiments were also done for Al_2O_3 with the same parameters as a control experiment. The metal concentration in the filtrate was estimated by using

https://doi.org/10.1021/acsomega.3c01609
ACS Omega 2023, 8, 17209−17219

Scheme 1. Schematic Representations of the Synthesis of Cu_2O NPs, Al_2O_3 NPs, and Cu_2O/Al_2O_3 Nanocomposite and Their Adsorption of Cd(II) from Aqueous Solution[a]

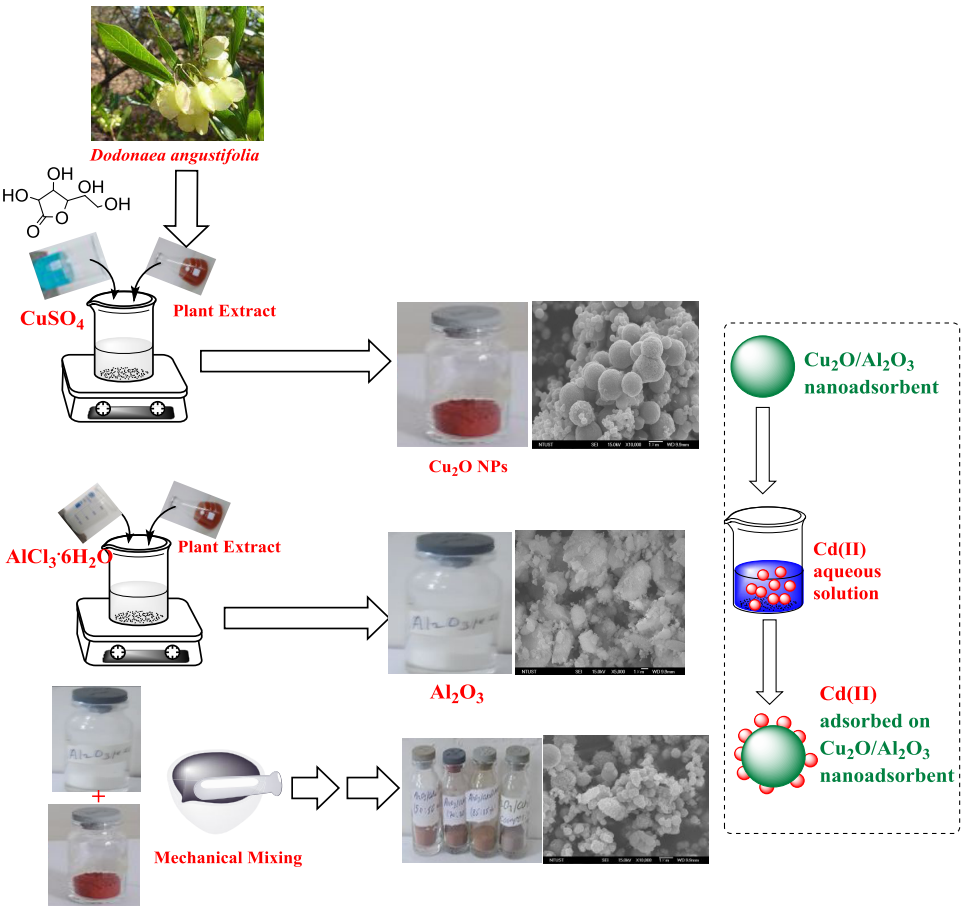

[a]Photos in figures are taken by Y.E.H. and the scheme was developed by W.M.G.

atomic absorption spectroscopy (AAS). The adsorption capacity as well as removal efficiency was calculated using eqs 1 and 2, respectively.

$$Q_e = \frac{(C_0 - C_e)}{W} \times V \quad (1)$$

$$R\ (\%) = \frac{(C_0 - C_e)}{C_0} \times 100 \quad (2)$$

Here, Q_e is the concentration of heavy metal ions adsorbed on the nanoadsorbent at equilibrium, R is percentage removal, V is the volume of metal ion solution in L, W is the weight of the adsorbent NPs in a gram scale, C_0 and C_e are the initial and equilibrium concentrations (in mg/L), respectively.

To investigate the effect of coexisting metal ions on the adsorptive removal of Cd(II) ions by the 5 %Cu_2O/Al_2O_3 nanocomposite material, 50 mg of selected metal ion precursor salts that are prevalent in normal and wastewater (Ca(II), Mg(II), Ni(II), Zn(II), Pb(II)) were mixed with 90 mg of the Cd(II) ion precursor. The combined metal salts were dissolved in 1 L of deionized water to give ∼140 mg/L (90 mg/L Cd + 50 mg/L additional competing ions) initial concentration. The resulting Cd−metal ion pair solutions were then analyzed for residual Cd(II) ions after being shaken for 60 min at the optimized pH (8.0) with the optimized composite adsorbent amount (0.3 g).

2.7. Characterization. The crystal phase of prepared NPs and nanocomposites was recognized using X-ray diffraction (XRD, Shimadzu XRD- 7000). Field emission scanning electron microscopy (FESEM, JSM 6500F, JEOL) was used to study the morphology of the nanomaterials. The surface functional groups of the nanomaterials were examined by using a 65 FT-IR (PerkinElmer) spectrometer. Nitrogen adsorption measurements were performed using the guest-free (evacuated) samples on a 3-Flex Surface Characterization Analyzer (Micromeritics) at pressures up to 1 bar. The surface areas of the materials were evaluated from the nitrogen adsorption isotherms collected at 77 K with the help of the Brunauer−Emmett−Teller (BET) model. Pore size distribution was analyzed using a BJH model from the desorption branch. A DW-AA320N atomic absorption spectrometer (AAS) was used for metal adsorption studies.

3. RESULTS AND DISCUSSION

3.1. Synthesis and Characterization. In this study, we report the first attempt at an eco-friendly approach for the plant extract-mediated synthesis of Cu_2O/Al_2O_3 nanocomposites. As illustrated in Scheme 1, *D. angustifolia* plant extract was employed as a reducing and stabilizing/capping agent for Al_2O_3 and Cu_2O NPs formation. During the formation of nanomaterials, precursors were thermally decomposed, and monomers accumulated in the solution during heat treatment.[24] Eruption nucleation occurred, while the monomer

https://doi.org/10.1021/acsomega.3c01609
ACS Omega 2023, 8, 17209−17219

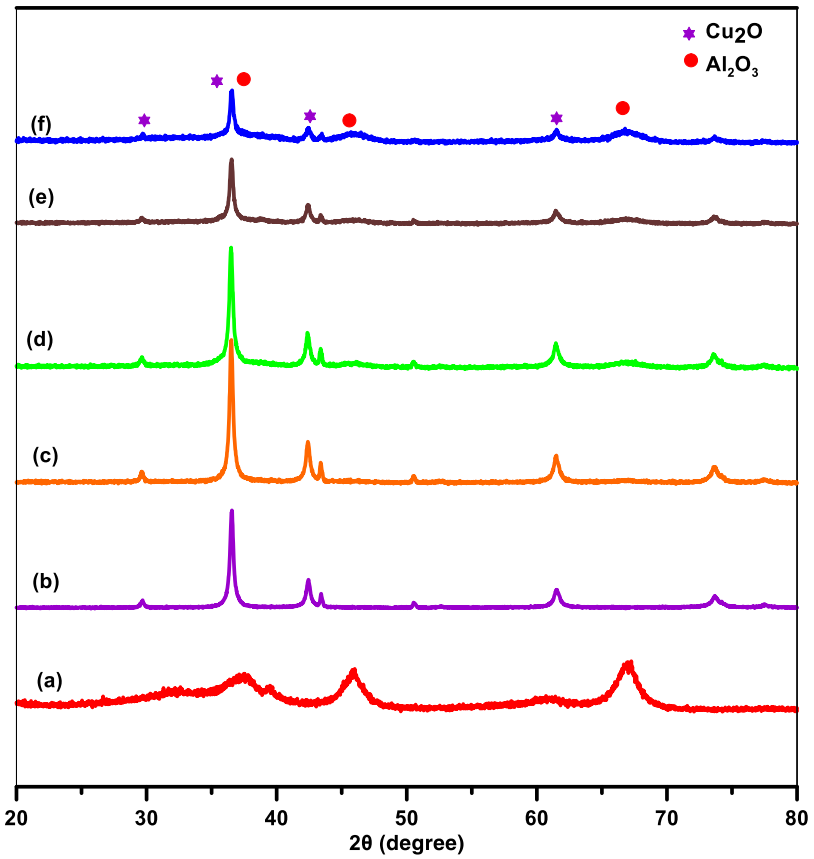

Figure 1. XRD patterns for (a) Al_2O_3, (b) Cu_2O, and (c) 50% Cu_2O/Al_2O_3, (d) 30% Cu_2O/Al_2O_3, (e) 15% Cu_2O/Al_2O_3, and (f) 5% Cu_2O/Al_2O_3.

concentration crossed a critical nucleation level, with the development of Al_2O_3 and Cu_2O NPs. After synthesis, white and brick-red precipitates indicated the formation of Al_2O_3 and Cu_2O NPs, respectively. Afterward, the nanocomposite was synthesized from the individual metal oxide powders by mixing with a mortar and pestle.

Figure 1a–f displays the XRD patterns of the prepared Al_2O_3 NPs, Cu_2O NPs, and Cu_2O/Al_2O_3 nanocomposites at different ratios. The XRD patterns revealed the orientation and crystalline nature of the synthesized nanocomposites. The major diffraction peaks of Cu_2O at 29.5, 36.5, 42.4, 61.5, and 73.6° belong to (110), (111), (200), (220), and (311) planes, respectively. These results agree well with the standard diffraction peaks of Cu_2O (JCPDS No. 05-0667).[25] Furthermore, the XRD peaks of Al_2O_3 are evident with (022), (122), (026), (220), (033), (232), and (042) planes at 32.5, 37.3, 39.3, 45.9, 47.9, 64.6, and 66.8°, respectively (Figure 1a,b). As shown in XRD patterns in Figure 1c–f, the Al_2O_3 peaks are shown clearly in the nanocomposites, particularly when decreasing the percentage of Cu_2O. The results demonstrate that the Cu_2O/Al_2O_3 nanocomposite was successfully synthesized without other impurity phases.

SEM micrographs of the as-synthesized Cu_2O, Al_2O_3, and 5% Cu_2O/Al_2O_3 nanocomposite are shown in Figure 2a–c, respectively. The SEM micrograph clearly showed no agglomerations of the nanostructure, and adhesion of NPs was found. The homogeneities with spherical morphologies of Cu_2O NPs were observed in SEM micrographs (Figure 2b). Consequently, the NPs are dispersed with two dissimilar structures on the entire surface homogeneously (Figure 2c). It can be observed that the surface of Al_2O_3 was covered by Cu_2O while preserving its morphology in the nanocomposites. According to EDS peaks, the existence of Al, Cu, and O was identified (Figure 2d). Furthermore, EDS demonstrates that Cu_2O NPs were embellished on the surface of Al_2O_3 NPs, as elemental monitoring using EDS investigation of the produced nanocomposite precisely displays all elemental combinations.

Figure 3a–d shows the FT-IR spectra of the plant extract, Al_2O_3, Cu_2O, and 5% Cu_2O/Al_2O_3 nanocomposite. The strong broad peak at 3300–3400 cm^{-1} is attributed to O–H groups of alcohols and phenols in plant extract as well as O–H groups from water molecules in all as-synthesized nanocomposites. The peak at 2914 cm^{-1} is allocated for C–H stretching vibrations in plant extract (Figure 3a). The stretching peaks at 1615, 1618, 1602, and 1625 cm^{-1} are attributed to C=C vibrations for plant extract and could indicate physisorbed water displayed in Al_2O_3, Cu_2O, and Cu_2O/Al_2O_3. The peaks that appear below 1400 cm^{-1} in nanocomposites are due to Al–O and Cu–O stretching vibrations (Figure 3d).[26,2726] The peak at 1362 cm^{-1} in plant extract belongs to the O–H bending vibration (Figure 3a). The peak that appears at 960 cm^{-1} is assigned to the bending vibrations of the Cu–O bond (Figure 3c).[28] The stretching peaks at 600 cm^{-1} (Figure 3b) and 590 cm^{-1} (Figure 3c) are assigned to Al–O and Cu–O, respectively.[29]

To verify the degree of porosity, pore size distribution, and surface area of the prepared Cu_2O/Al_2O_3 nanocomposite, an adsorption experiment was carried out at 77 K using N_2 as a probe molecule. The N_2 sorption isotherms of the nanocomposite adsorbent exhibited a fully reversible type-IV

https://doi.org/10.1021/acsomega.3c01609
ACS Omega 2023, 8, 17209–17219

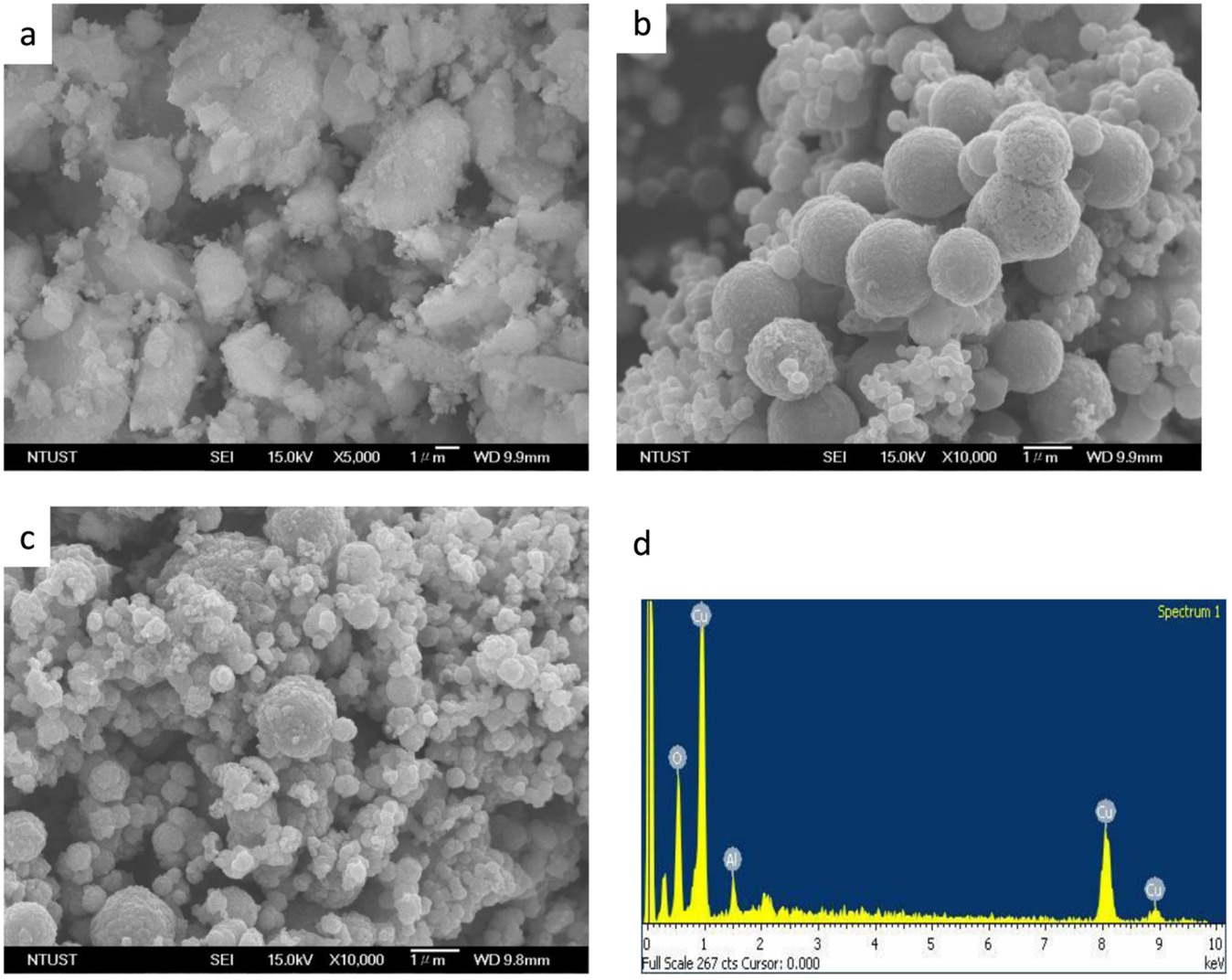

Figure 2. SEM images for (a) Al_2O_3, (b) Cu_2O, and (c) 5%Cu_2O/Al_2O_3. (d) SEM EDS of 5% Cu_2O/Al_2O_3.

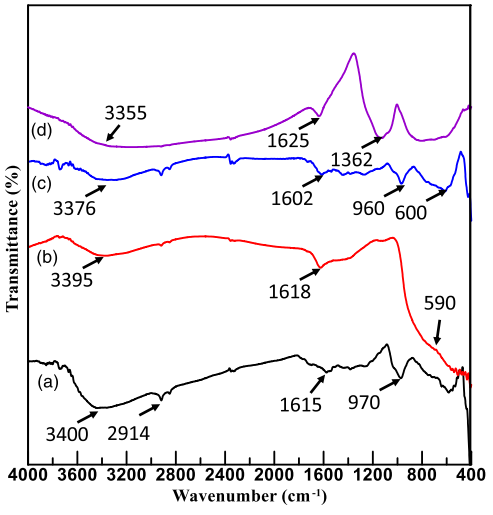

Figure 3. FT-IR spectra of (a) *D. angustifolia* plant extract (b) Al_2O_3, (c) Cu_2O, and (d) 5% Cu_2O/Al_2O_3 nanocomposite.

isotherm (Figure 4), a characteristic of a mesoporous material with a BET area of 172 $m^2\ g^{-1}$ and a pore volume of 0.45 $cm^3\ g^{-1}$ at P/P_0 ~0.95. The pore size distribution for the nanocomposite was deduced from the N_2 sorption data using the BJH desorption model. It revealed one type of uniform mesopores with an average size centered around 6 nm. The characteristic hysteresis loop of a typical mesoporous material of uniform pores, resulting from capillary condensation of the adsorbate, is also clearly evident in the isotherm.

3.2. Adsorption Studies. *3.2.1. Effect of pH.* The pH of the solution is the foremost controlling parameter in the effectiveness of the adsorption procedure because it alters the surface charge of the adsorbent via protonation or deprotonation. The removal efficiency of Cd(II) by $A1_2O_3$ and Cu_2O/Al_2O_3 was tested at different selected pH values (2−10), with adsorbent dose = 0.3 g, contact time = 60 min, and initial concentration of Cd(II) = 0.2 mg/L (Figure 5a). The effectiveness of Cd adsorption relied on the protonation as well as deprotonation of the surface functional groups of the nanocomposite.[30] The maximum removal efficiency for Cd(II) by $A1_2O_3$ and Cu_2O/Al_2O_3 was observed at a pH value of 8, which is 87.77 and 96.17%, respectively (Figure 5a). At lower pH values, both Al_2O_3 and Cu_2O/Al_2O_3 nanocomposites showed less Cd(II) affinity. Cd(II) ions could be present in deionized water during the Cd(II) adsorption process in the form of Cd^{2+}, $[Cd(H_2O)_6]^{2+}$, $Cd(OH)^+$, and $Cd(OH)_2(s)$, although at a lower pH, $[Cd(H_2O)_6]^{2+}$ is the dominant ion

https://doi.org/10.1021/acsomega.3c01609
ACS Omega 2023, 8, 17209−17219

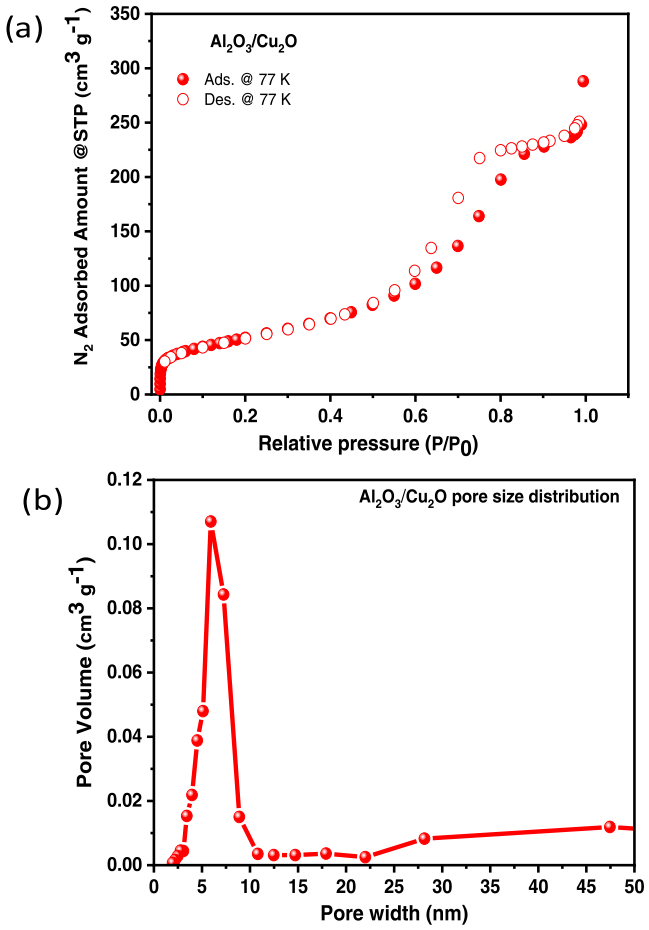

Figure 4. BET (a) N_2 adsorption−desorption isotherm and (b) pore size distribution for the 5% Cu_2O/Al_2O_3 nanoadsorbent.

that could be adsorbed by the Al_2O_3 or Cu_2O/Al_2O_3 nanocomposite.[31] Owing to the presence of hydroxide (OH^-) ions in the adsorption solution, Cd precipitation in the form of $Cd(OH)_2$ could occur when the initial pH of the Cd solutions was raised to high values. According to the findings of other studies, the maximum Cd removal typically took place in the pH range of 4−8 (weakly acidic and neutral), which is consistent with the findings of the current study.[32] The studies by Asgari et al. saw the greatest Cd removal at pH 7.[33]

3.2.2. Effect of Adsorbent Amount. To investigate the effects of adsorbent (nanocomposite) dosage, different quantities of the adsorbent ranging from 0.1 to 0.4 g were used in the batch experiment. The other parameters, i.e., a pH of 8, a contact time of 60 min, and an initial Cd(II) concentration of 0.2 mg/L, were used to optimize the optimum amount of the adsorbent. The percentage removal efficiencies of Cd(II) by $A1_2O_3$ and Cu_2O/Al_2O_3 are displayed in Figure 5b. The adsorption eradication efficiency improved from 81.63 to 89.50% for $A1_2O_3$ and from 91.89 to 96.62% for Cu_2O/Al_2O_3 when the adsorbent amount varied from 0.1 to 0.3 g. However, approximately constant removal efficiency was noted upon further increasing the adsorbent dosage to 0.4 g. The increase in the removal efficiency as the amount increases is attributed to the availability of a greater number of accessible adsorption sites at the higher dosage.[34] Remaining unsaturated during the adsorption reaction, as a result of a greater number of available adsorption sites favoring Cd (II) uptake. The slightly constant adsorption efficiency at adsorbent dosage >0.3 g at the set initial Cd(II) concentration could be attributed to the consumption of the available Cd(II) in the solution.

3.2.3. Effects of Cd(II) Initial Concentrations. Four different concentrations such as 30, 60, 90, and 120 mg/L of Cd(II) were prepared and tested to examine the influence on the removal efficiency at pH = 8, contact time = 60 min, and adsorbent dose = 0.3 g. As shown in Figure 5c, the removal efficiency of both (Al_2O_3 and Cu_2O/Al_2O_3) adsorbents increased with increasing concentration of Cd(II). The percentage removal effectiveness of Cd(II) by Al_2O_3 and Cu_2O/Al_2O_3 enhanced from 85.86 to 89.49% and 88.29 to 95.40%, respectively (Figure 5c), with increasing starting concentration from 30 to 90 mg/L. Indeed, increasing concentration can act as a driving force in resolving all-mass transfer encounters from the aqueous to the solid phase. The adsorption of Pb(II), Cd(II), Ni(II), and Cu(II) by modified Fe_3O_4 yielded similar results.[35] The highest removal percent was found at 90 mg/L and slightly decreased as the initial concentration of Cd(II) further increased to 120 mg/L. This could be due to limited adsorption sites in the adsorbent material. Since a fixed quantity of the adsorbent is used, the sites become saturated at a certain concentration, making the saturated adsorbent incapable of absorbing any more Cd-(II).[30,33,36]

3.2.4. Effect of Contact Time. The effect of contact time on the elimination of Cd(II) by Al_2O_3 and Cu_2O/Al_2O_3 was investigated at a pH of 8, an adsorbent dose of 0.3 g, and an initial Cd(II) concentration of 90 mg/L. The contact time was varied from 30 to 120 min at a temperature of 25 °C. Figure 5d shows the removal efficiency of Cd(II) by Al_2O_3 and Cu_2O/Al_2O_3, with an increase in % removal from 73.61 to 89.62% and 92.61 to 97.36%, respectively, upon increasing the contact time from 30 to 90 min for Al_2O_3 and from 30 to 60 min for Cu_2O/Al_2O_3.

The removal efficiency was fast at the start of the adsorption process, achieving 97.36% and then reaching nearly a plateau later on. The primary cause of this behavior is the saturation of the active sites in the nanocomposite, which prevents further Cd(II) adsorption. This property is described by the fact that the total number of adsorption sites on the surface of the nanocomposite is initially very high, making adsorption very quick; however, over time, the active sites become saturated, minimizing the adsorption rate.[37] In all factors of adsorption parameters, the nanocomposite showed better adsorption behavior, which could be due to the high surface area.

3.2.5. Effect of Coexisting Metal Ions. Besides Cd(II) ions, many metal ions coexist in wastewater. Adsorption studies in the presence of coexisting metal ions are thus necessary to determine the effect of competing ions on removal efficiency. As a result, the effects of extra metal ions on Cd(II) removal efficiency by the 5% Cu_2O/Al_2O_3 nanocomposite were investigated. The percent removal efficiency of Cd(II) ions by the composite material with and without Mg(II), Ca(II), Ni(II), Zn(II), and Pb(II) metal ions is shown in Figure 6. The coexisting metal ions were found to influence the percentage removal of Cd(II) at different extents, with Ni(II) having a significant effect. The observed interference order shows some degree of correlation with the charge density (charge/radius ratio) values of metal ions:[38] Ni^{2+} (2/0.70) > Zn^{2+} > (2/0.74) ≈ Mg^{2+} (2/0.72) > Ca^{2+} (2/1.23) ≈ Pb^{2+} (2/1.19). The negligible impact of Pd(II) and Ca(II) ions on the removal efficiency of Cd(II) could be attributed to the preferential

https://doi.org/10.1021/acsomega.3c01609
ACS Omega 2023, 8, 17209−17219

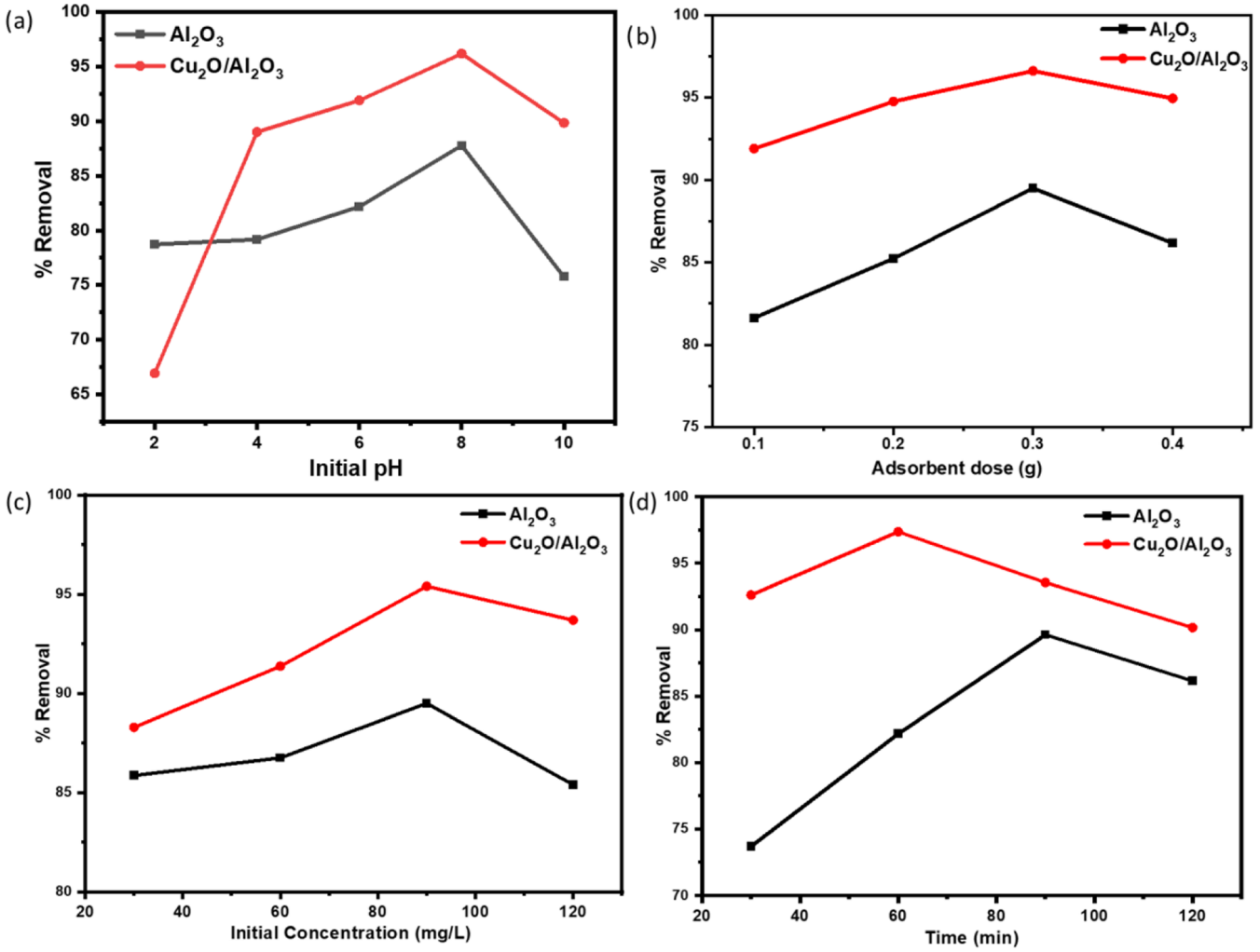

Figure 5. Effect of (a) initial pH (b), adsorbent dose, (c) initial concentration of Cd(II), and (d) contact time on the removal efficiency of Cd(II) by Al_2O_3 NPs and the 5% Cu_2O/Al_2O_3 nanocomposite.

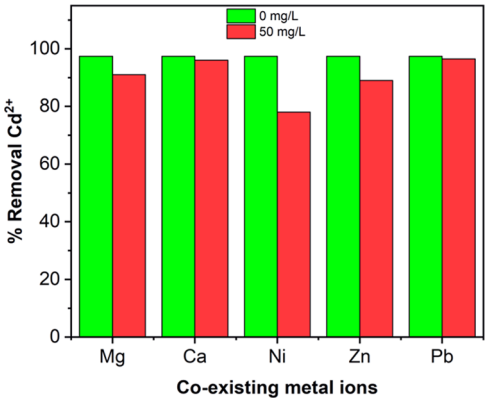

Figure 6. Effect of competing metal ions on Cd(II) removal efficiency by the 5% Cu_2O/Al_2O_3 nanocomposite.

adsorption of the Cd(II) ions with a higher charge density (2/0.95) on the adsorption sites of the adsorbent. The adsorbed Cd ions could then repel the incoming competing ions.

3.3. Kinetic Study. One of the key considerations when designing an adsorption system is the prediction of the adsorption procedure. The kinetics of Cd adsorption on Al_2O_3 and the Cu_2O/Al_2O_3 nanocomposite was scrutinized using various kinetic models such as pseudo-first-order and second-order models (eqs 3 and 4) at an initial concentration of 90 mg/L.

$$\ln(q_e - q_t) = \ln q_e - k_1 t \quad (3)$$

$$t/q_t = 1/k_2 q^2 e + 1/q_e t \quad (4)$$

where q_t and q_e (mg/g) are the values of absorbed Cd^{2+} at t and equilibrium, respectively. k_1 (1/min) and k_2 (g/(mg·min)) are the rate constants of the first-order and second-order models, respectively.

The adsorption experiment of ions was performed at different contact times (30, 60, 90, and 120 min) with an initial concentration of 30 mg/L for the kinetic study. According to Figure 6, equilibrium is reached after 90 min of contact time for Al_2O_3 NPs and 60 min for the Cu_2O/Al_2O_3 nanocomposite. The kinetics of adsorption of Cd(II) by the adsorbent were studied, and the experimental data obtained were applied to pseudo-first-order as well as pseudo-second-order kinetic models.

The outcomes of the kinetic study are summarized in Table 1 and Figure 7a–d. Figure 7 shows that the most appropriate kinetic model to explain the adsorption procedure is the pseudo-second-order kinetic model along with a correlation

https://doi.org/10.1021/acsomega.3c01609
ACS Omega 2023, 8, 17209−17219

Table 1. Parameters of the Kinetic Models for the Adsorption of Cd(II) Ions Using Al_2O_3 and Cu_2O/Al_2O_3 Nanoadsorbents

pseudo-first-order				
	q_e exp (mg/g)	q_e cal (mg/g)	k_1	R^2
Al_2O_3	0.019339	62.92	1.89	0.7127
Cu_2O/Al_2O_3	0.2207	3495	0.0002	0.573
pseudo-second-order				
	q_e exp (mg/g)	q_e cal (mg/g)	k_2	R^2
Al_2O_3	0.019339	0.232	0.597	0.995
Cu_2O/Al_2O_3	0.2207	0.2215	1.391	0.998

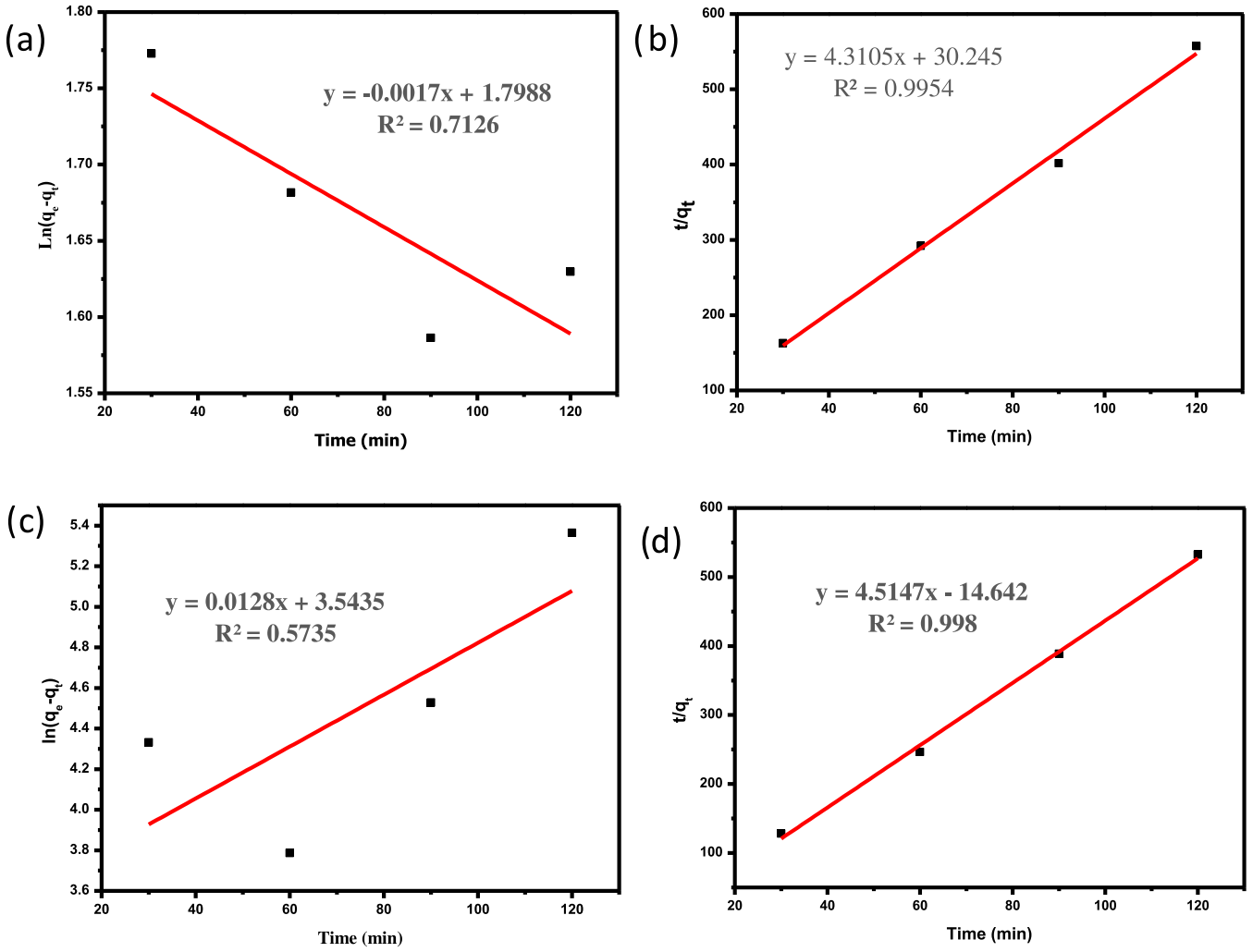

Figure 7. (a) Pseudo-first-order kinetics for Al_2O_3, (b) pseudo-second-order kinetics for Al_2O_3, (c) pseudo-first-order kinetics for Cu_2O/Al_2O_3, and (d) pseudo-second-order kinetics for Cu_2O/Al_2O_3 for the adsorption of Cd(II) at room temperature.

coefficient (R^2) of 0.998, and the estimated adsorption capacity (q_e cal) is in perfect agreement with the experimental data (q_e exp; Table 1).

3.4. Isotherm Study. Typically, the dispersion of heavy metal ions among the liquid phase as well as the solid phase at equilibrium is demonstrated by the adsorption isotherm.[39] In addition, to explain the mechanism of Cd(II) adsorption, the Langmuir model (eq 5) and the widely used empirical Freundlich model (eqs 6 and 7) were used. The Freundlich model is valid for sorption on a nonhomogeneous surface and demonstrates multilayer adsorption.[32,33]

$$q_e = \frac{q_m K_L c_e}{1 + K_L c_e} \quad (5)$$

$$q_e = K_F c_e^{1/n} \quad (6)$$

$$\ln q_e = \ln K_F + \frac{1}{n} \ln c_e \quad (7)$$

where the highest monolayer adsorption capacity is indicated by q_m (mg/g), K_L indicates the constant of the Langmuir equation, which is correlated to the energy of adsorption (L/g), q_e is the quantity of Cd(II) adsorbed on the surface of the nanocomposite at equilibrium in mg/g, K_F is the Freundlich isotherm constant in L/mg, n = adsorption capacity, and c_e is

https://doi.org/10.1021/acsomega.3c01609
ACS Omega 2023, 8, 17209−17219

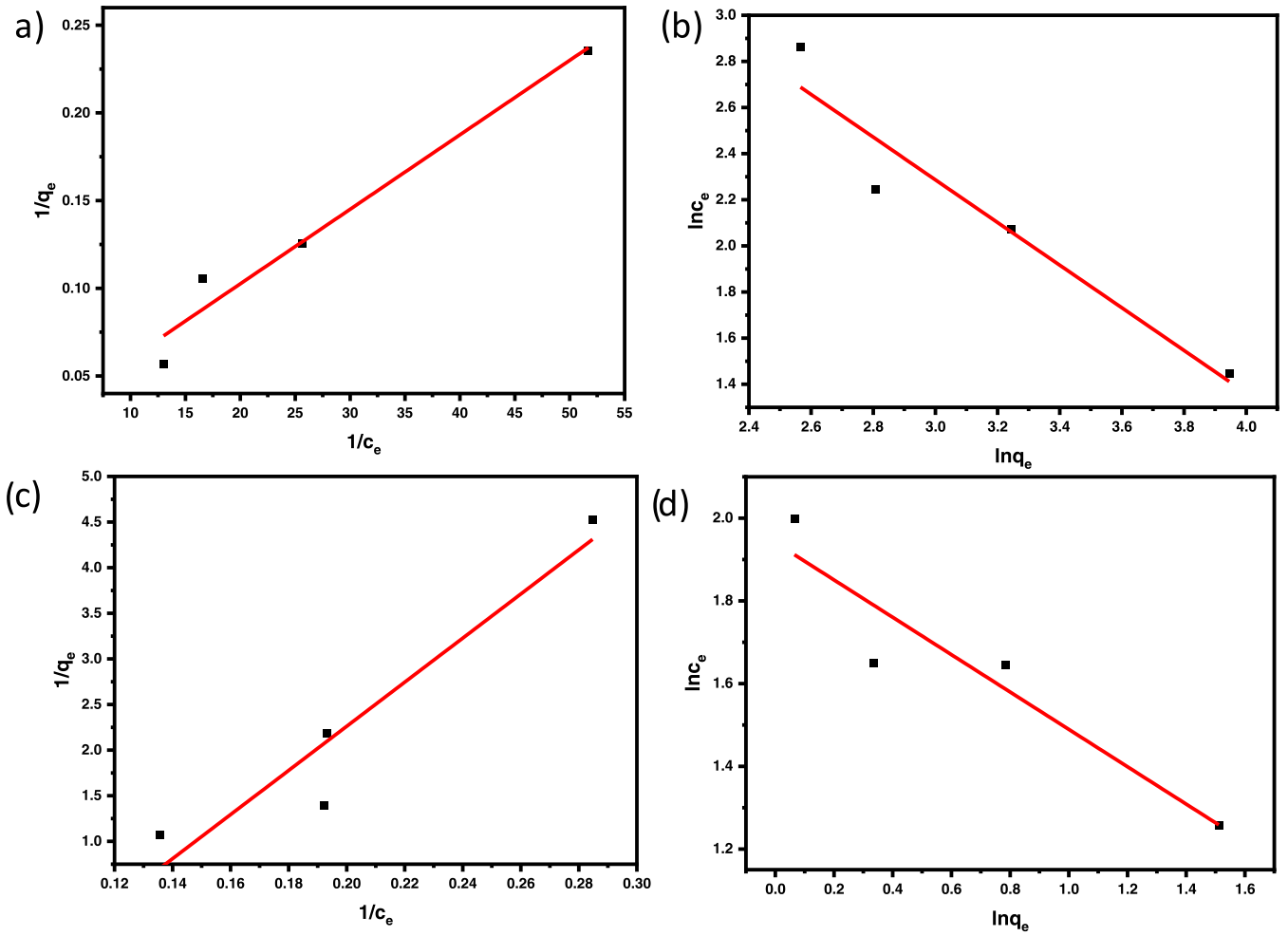

Figure 8. (a) Langmuir isotherm for Al_2O_3, (b) Freundlich isotherm for Al_2O_3, (c) Langmuir isotherm for Cu_2O/Al_2O_3, and (d) Freundlich isotherm for Cu_2O/Al_2O_3 for the adsorption of Cd (II) at room temperature.

Table 2. Parameters of Langmuir and Freundlich Isotherm Models for Cd(II) Ion Removal Using Al_2O_3 and Cu_2O/Al_2O_3 Nanoadsorbents

	Langmuir isotherm				Freundlich isotherm		
parameter	q_m	K_L	R_L	R^2	n	K_F	R^2
Al_2O_3	0.3204	0.0137	0.448	0.9666	1.081	115.080	0.9217
Cu_2O/Al_2O_3	26.525	1	0.011	0.9116	0.213	87.297	0.8887

the equilibrium concentration of Cd(II) in mg/L. Figure 8a–d and Table 2 show the Cd(II) ion sorption isotherms on Al_2O_3 NPs and the Cu_2O/Al_2O_3 nanocomposite. A better linear plot is obtained from Figure 8a,c, indicating that the adsorption of Cd(II) ions by Al_2O_3 and the Cu_2O/Al_2O_3 nanocomposite may be admirably explained by the Langmuir isotherm model. Furthermore, for both NPs (R^2 = 0.9666) and (R^2 = 0.9116), the linear correlation coefficient of the Langmuir isotherm model was the highest among Freundlich isotherm models. Table 2 demonstrates that the Langmuir adsorption model is the best fit for Cd(II) adsorption onto Al_2O_3 and the Cu_2O/Al_2O_3 nanocomposite, assuming that Cd(II) removal occurs on a homogeneous monolayer, equivalent adsorption energy, uniform active sites, and no interactions between the adsorbed species.[40] The theoretical maximal eradication capacities (q_m) of Al_2O_3 and Cu_2O/Al_2O_3 calculated by the Langmuir isotherm model were 0.3204 and 26.525 mg/g, respectively, which were greater than q_e exp (mg/g), indicating that the process was monolayer adsorption and the adsorption surface was not completely covered.[41] Adsorption cannot be reversed if the dimensionless separation factor (R_L) = 0. When R_L is between 0 and 1, the process is advantageous. If the value of R_L equals 1, the isotherm is linear. If R_L is greater than 1, an unfavorable process is in control. A dimensionless equilibrium parameter or separation factor, R_L, was reported by researchers as a crucial parameter of the Langmuir isotherm for predicting whether an adsorption system will be beneficial or detrimental.[42] The R_L was calculated as 0.448 and 0.011 L/mg (Table 2) for Al_2O_3 and Cu_2O/Al_2O_3, respectively, which lie between 0 and 1, indicating that the adsorption of Cd(II) onto Al_2O_3 and Cu_2O/Al_2O_3 nanoadsorbents was favorable, as experimentally survived, signifying the outstanding adsorption behavior of the Cu_2O/Al_2O_3 nanocomposite, which is anticipated to play a vital role in polluted water treatment applications.

https://doi.org/10.1021/acsomega.3c01609
ACS Omega 2023, 8, 17209−17219

4. CONCLUSIONS

In the current study, the Cu_2O/Al_2O_3 nanocomposite was fruitfully synthesized by a green synthesis method using *D. angustifolia* plant extract as a reducing, protecting, and stabilizing agent. The crystallite and morphologies of nanocomposites were studied by XRD and SEM analysis. The porosity attributes (surface area, pore size distribution, and pore volume) were analyzed by collecting N_2 adsorption−desorption isotherms at 77 K, and the obtained nanocomposite has a high surface area with a mesoporous structure. According to the results, the Cu_2O/Al_2O_3 nanocomposite was effectually employed for the adsorption of Cd^{2+} ions from aqueous solutions. Furthermore, Cd(II) ion adsorption onto the nanocomposite was demonstrated to be pH-dependent. The influence of initial Cd concentration, contact time, and nanocomposite quantity on adsorption potentiality was thoroughly investigated. The adsorption rates of the Cu_2O/Al_2O_3 nanocomposite were very rapid, and adsorption equilibria were attained in 60 min for 97.36% removal of Cd(II) from aqueous solutions. With a highest adsorption capacity of 4.48 mg/g, the adsorption data closely fitted to the pseudo-second-order kinetics and Langmuir isotherm models. Therefore, the synthesized Cu_2O/Al_2O_3 nanocomposite could be a potential candidate for the vastly effectual adsorptive removal of heavy metal ions.

AUTHOR INFORMATION

Corresponding Author

Wubshet Mekonnen Girma − *Department of Chemistry, College of Natural Science, Wollo University, Dessie 1000, Ethiopia;* orcid.org/0000-0003-3370-6731; Phone: +251-910804026; Email: wubshet.mekonnen@wu.edu.et

Authors

Yeshi Endris Hassen − *Department of Chemistry, College of Natural Science, Wollo University, Dessie 1000, Ethiopia*

Gangaraju Gedda − *Department of Chemistry, School of Engineering, Presidency University, Bangalore 560064 Karnataka, India*

Ayalew H. Assen − *Department of Chemistry, College of Natural Science, Wollo University, Dessie 1000, Ethiopia*

Daniel Manaye Kabtamu − *Department of Chemistry, Debre Berhan University, Debre Berhan 7260, Ethiopia; Department of Materials Science and Engineering, National Taiwan University of Science and Technology, Taipei 10607, Taiwan*

Complete contact information is available at: https://pubs.acs.org/10.1021/acsomega.3c01609

Notes

The authors declare no competing financial interest.

ACKNOWLEDGMENTS

The authors would like to thank Wollo University for funding. The authors also would like to gratefully acknowledge the National Taiwan Science and Technology University for SEM imaging and Adama Science and Technology University for XRD analysis.

REFERENCES

(1) (a) Al Maashri, A.; Pathuri, L.; Awadalla, M.; Ahmad, A.; Ould-Khaoua, M. Optimized hardware crypto engines for XTEA and SHA-512 for wireless sensor nodes. *Indian J. Sci. Technol.* **2016**, *9*, 90026. (b) Gupta, B.; Mishra, A.; Singh, R.; Thakur, I. S. Fabrication of calcite based biocomposites for catalytic removal of heavy metals from electroplating industrial effluent. *Environ. Technol. Innovation* **2021**, *21*, 101278.

(2) (a) Alyasi, H.; Mackey, H. R.; Loganathan, K.; McKay, G. Adsorbent minimisation in a two-stage batch adsorber for cadmium removal. *J. Ind. Eng. Chem.* **2020**, *81*, 153−160. (b) Qamar, M.; Gondal, M.; Yamani, Z. Synthesis of nanostructured NiO and its application in laser-induced photocatalytic reduction of Cr (VI) from water. *J. Mol. Catal. A* **2011**, *341*, 83−88. (c) Shahryari, T.; Mostafavi, A.; Afzali, D.; Rahmati, M. Enhancing cadmium removal by low-cost nanocomposite adsorbents from aqueous solutions; a continuous system. *Composites, Part B* **2019**, *173*, 106963.

(3) Singh, H.; Rana, S.; Mittal, S. Experimental investigation and kinetic modeling of adsorption behaviour of inexpensive Ziziphus mauritiana seeds. *Indian J. Chem. Technol.* **2018**, *24*, 488−497.

(4) Joo, J. B.; Park, J.; Yi, J. Preparation of polyelectrolyte-functionalized mesoporous silicas for the selective adsorption of anionic dye in an aqueous solution. *J. Hazard. Mater.* **2009**, *168*, 102−107.

(5) Meshko, V.; Markovska, L.; Mincheva, M.; Rodrigues, A. Adsorption of basic dyes on granular acivated carbon and natural zeolite. *Water Res.* **2001**, *35*, 3357−3366.

(6) Herrera-Barros, A.; Tejada-Tovar, C.; Villabona-Ortíz, A.; Gonzalez-Delgado, A.; Benitez-Monroy, J. Cd (II) and Ni (II) uptake by novel biosorbent prepared from oil palm residual biomass and Al2O3 nanoparticles. *Sustainable Chem. Pharm.* **2020**, *15*, No. 100216.

(7) Patra, A. K.; Das, S. K.; Bhaumik, A. Self-assembled mesoporous TiO 2 spherical nanoparticles by a new templating pathway and its enhanced photoconductivity in the presence of an organic dye. *J. Mater. Chem.* **2011**, *21*, 3925−3930.

(8) Zhang, C.; Wang, W.; Duan, A.; Zeng, G.; Huang, D.; Lai, C.; Tan, X.; Cheng, M.; Wang, R.; Zhou, C.; et al. Adsorption behavior of engineered carbons and carbon nanomaterials for metal endocrine disruptors: Experiments and theoretical calculation. *Chemosphere* **2019**, *222*, 184−194.

(9) Kong, Q.; Shi, X.; Ma, W.; Zhang, F.; Yu, T.; Zhao, F.; Zhao, D.; Wei, C. Strategies to improve the adsorption properties of graphene-based adsorbent towards heavy metal ions and their compound pollutants: A review. *J. Hazard. Mater.* **2021**, *415*, No. 125690.

(10) Dehghani, M. H.; Yetilmezsoy, K.; Salari, M.; Heidarinejad, Z.; Yousefi, M.; Sillanpää, M. Adsorptive removal of cobalt (II) from aqueous solutions using multi-walled carbon nanotubes and γ-alumina as novel adsorbents: Modelling and optimization based on response surface methodology and artificial neural network. *J. Mol. Liq.* **2020**, *299*, No. 112154.

(11) You, J.; Zhao, Y.; Wang, L.; Bao, W.; He, Y. Atomic layer deposition of γ-Fe2O3 nanoparticles on modified MWCNT for efficient adsorption of Cr (VI) ions from aqueous solution. *J. Phys. Chem. Solids* **2020**, *142*, No. 109441.

(12) (a) Jung, K.-W.; Lee, S. Y.; Choi, J.-W.; Lee, Y. J. A facile one-pot hydrothermal synthesis of hydroxyapatite/biochar nanocomposites: adsorption behavior and mechanisms for the removal of copper (II) from aqueous media. *Chem. Eng. J.* **2019**, *369*, 529−541. (b) Chatterjee, S.; Bhanja, P.; Ghosh, D.; Kumar, P.; Kanti Das, S.; Dalapati, S.; Bhaumik, A. Metformin-templated nanoporous ZnO and covalent organic framework heterojunction photoanode for photoelectrochemical water oxidation. *ChemSusChem* **2021**, *14*, 408−416.

(13) Huang, J.; Li, Q.; Sun, D.; Lu, Y.; Su, Y.; Yang, X.; Wang, H.; Wang, Y.; Shao, W.; He, N.; et al. Biosynthesis of silver and gold nanoparticles by novel sundried Cinnamomum camphora leaf. *Nanotechnology* **2007**, *18*, No. 105104.

(14) Zou, S. J.; Ding, B. H.; Chen, Y. F.; Fan, H. T. Nanocomposites of graphene and zirconia for adsorption of organic-arsenic drugs:

Performances comparison and analysis of adsorption behavior. *Environ. Res.* **2021**, *195*, No. 110752.
(15) Oyewo, O. A.; Elemike, E. E.; Onwudiwe, D. C.; Onyango, M. S. Metal oxide-cellulose nanocomposites for the removal of toxic metals and dyes from wastewater. *Int. J. Biol. Macromol.* **2020**, *164*, 2477−2496.
(16) Jiang, Y.; Mao, Q.; Ma, T.; Liu, X.; Li, Y.; Ren, S.; Sun, J. Facile preparation of Fe2O3 Al2O3 composite with excellent adsorption properties towards Congo red. *Ceram. Int.* **2021**, *47*, 13884−13894.
(17) Joshi, N. C.; Malik, N.; Singh, A. Synthesis and characterizations of polythiophene−Al2O3 based nanosorbent and its applications in the removal of Pb2+, Cd2+ and Zn2+ ions. *J. Inorg. Organomet. Polym. Mater.* **2020**, *30*, 1438−1447.
(18) Joshi, N. C.; Negi, S. Synthesis and adsorption potential of an organic−inorganic-based hybrid nanomaterial (PANI-Al2O3). *Inorg. Nano-Met. Chem.* **2022**, *52*, 451−460.
(19) Razmgar, K.; Saljoughi, E.; Mousavi, S. M. Preparation and characterization of a novel hydrophilic PVDF/PVA/Al2O3 nanocomposite membrane for removal of As (V) from aqueous solutions. *Polym. Compos.* **2019**, *40*, 2452−2461.
(20) Mohammed, A. M.; Mohtar, S. S.; Aziz, F.; Aziz, M.; Ul-Hamid, A. Cu2O/ZnO-PANI ternary nanocomposite as an efficient photocatalyst for the photodegradation of Congo Red dye. *J. Environ. Chem. Eng.* **2021**, *9*, No. 105065.
(21) Guo, X.; Xu, Y.; Zha, F.; Tang, X.; Tian, H. α-Fe2O3/Cu2O (SO4) composite as a novel and efficient heterogeneous catalyst for photo-Fenton removal of Orange II. *Appl. Surf. Sci.* **2020**, *530*, No. 147144.
(22) Botsa, S. M.; Basavaiah, K. Fabrication of multifunctional TANI/Cu2O/Ag nanocomposite for environmental abatement. *Sci. Rep.* **2020**, *10*, No. 14080.
(23) (a) Behera, M.; Giri, G. Inquiring the photocatalytic activity of cuprous oxide nanoparticles synthesized by a green route on methylene blue dye. *Int. J. Ind. Chem.* **2016**, *7*, 157−166. (b) Kangralkar, M. V.; Kangralkar, V. A.; Manjanna, J. Adsorption of Cr (VI) and photodegradation of rhodamine b, rose bengal and methyl red on Cu2O nanoparticles. *Environ. Nanotechnol., Monit. Manage.* **2021**, *15*, 100417.
(24) Reiss, P.; Carriere, M.; Lincheneau, C.; Vaure, L.; Tamang, S. Synthesis of Semiconductor Nanocrystals, Focusing on Nontoxic and Earth-Abundant Materials. *Chem. Rev.* **2016**, *116*, 10731−10819.
(25) (a) Long, J.; Dong, J.; Wang, X.; Ding, Z.; Zhang, Z.; Wu, L.; Li, Z.; Fu, X. Photochemical synthesis of submicron- and nano-scale Cu2O particles. *J. Colloid Interface Sci.* **2009**, *333*, 791−799 10.1016/j.jcis.2009.02.036.. (b) He, Q.; Tian, Y.; Wu, Y.; Liu, J.; Li, G.; Deng, P.; Chen, D. Electrochemical Sensor for Rapid and Sensitive Detection of Tryptophan by a Cu(2)O Nanoparticles-Coated Reduced Graphene Oxide Nanocomposite. *Biomolecules* **2019**, *9*, 176.
(26) Boumaza, A.; Favaro, L.; Lédion, J.; Sattonnay, G.; Brubach, J.; Berthet, P.; Huntz, A.; Roy, P.; Tétot, R. Transition alumina phases induced by heat treatment of boehmite: an X-ray diffraction and infrared spectroscopy study. *J. Solid State Chem.* **2009**, *182*, 1171−1176.
(27) Xu, B.; Yang, Y.; Xu, Y.; Han, B.; Wang, Y.; Liu, X.; Yan, Z. Synthesis and characterization of mesoporous Si-modified alumina with high thermal stability. *Microporous Mesoporous Mater.* **2017**, *238*, 84−89.
(28) Jun-Cheng, L.; Lan, X.; Feng, X.; Zhan-Wen, W.; Fei, W. Effect of hydrothermal treatment on the acidity distribution of γ-Al2O3 support. *Appl. Surf. Sci.* **2006**, *253*, 766−770.
(29) Nasrollahzadeh, M.; Issaabadi, Z.; Sajadi, S. M. Green synthesis of Cu/Al2O3 nanoparticles as efficient and recyclable catalyst for reduction of 2, 4-dinitrophenylhydrazine, Methylene blue and Congo red. *Composites, Part B* **2019**, *166*, 112−119.
(30) Safari, M.; Rezaee, R.; Soltani, R. D. C.; Asgari, E. Dual immobilization of magnetite nanoparticles and biosilica within alginate matrix for the adsorption of Cd (II) from aquatic phase. *Sci. Rep.* **2022**, *12*, No. 11473.
(31) Tan, Y.; Chen, M.; Hao, Y. High efficient removal of Pb (II) by amino-functionalized Fe3O4 magnetic nano-particles. *Chem. Eng. J.* **2012**, *191*, 104−111.
(32) Tabesh, S.; Davar, F.; Loghman-Estarki, M. R. Preparation of γ-Al2O3 nanoparticles using modified sol-gel method and its use for the adsorption of lead and cadmium ions. *J. Alloys Compd.* **2018**, *730*, 441−449.
(33) Safari, M.; Rezaee, R.; Soltani, R. D. C.; Asgari, E. Dual immobilization of magnetite nanoparticles and biosilica within alginate matrix for the adsorption of Cd (II) from aquatic phase. *Sci. Rep.* **2022**, *12*, No. 11473.
(34) Haso, H. W.; Dubale, A. A.; Chimdesa, M. A.; Atlabachew, M. High Performance Copper Based Metal Organic Framework for Removal of Heavy Metals From Wastewater. *Front. Mater.* **2022**, *9*, No. 840806.
(35) Xue, S.; Xiao, Y.; Wang, G.; Fan, J.; Wan, K.; He, Q.; Gao, M.; Miao, Z. Adsorption of heavy metals in water by modifying Fe3O4 nanoparticles with oxidized humic acid. *Colloids Surf., A* **2021**, *616*, No. 126333.
(36) (a) Behnajady, M. A.; Yavari, S.; Modirshahla, N. Investigation on adsorption capacity of TiO2-P25 nanoparticles in the removal of a mono-azo dye from aqueous solution: a comprehensive isotherm analysis. *Chem. Ind. Chem. Eng. Q.* **2014**, *20*, 97−107. (b) Chowdhury, S.; Mishra, R.; Saha, P.; Kushwaha, P. Adsorption thermodynamics, kinetics and isosteric heat of adsorption of malachite green onto chemically modified rice husk. *Desalination* **2011**, *265*, 159−168.
(37) Yagub, M. T.; Sen, T. K.; Afroze, S.; Ang, H. M. Dye and its removal from aqueous solution by adsorption: a review. *Adv. Colloid Interface Sci.* **2014**, *209*, 172−184.
(38) Tansel, B. Significance of thermodynamic and physical characteristics on permeation of ions during membrane separation: Hydrated radius, hydration free energy and viscous effects. *Sep. Purif. Technol.* **2012**, *86*, 119−126.
(39) Langmuir, I. The adsorption of gases on plane surfaces of glass, mica and platinum. *J. Am. Chem. Soc.* **1918**, *40*, 1361−1403.
(40) Zheng, S.; Hao, L.; Zhang, L.; Wang, K.; Zheng, W.; Wang, X.; Zhou, X.; Li, W.; Zhang, L. Tea polyphenols functionalized and reduced graphene oxide-ZnO composites for selective Pb2+ removal and enhanced antibacterial activity. *J. Biomed. Nanotechnol.* **2018**, *14*, 1263−1276.
(41) Oskui, F. N.; Aghdasinia, H.; Sorkhabi, M. G. Adsorption of Cr (III) using an Iranian natural nanoclay: applicable to tannery wastewater: equilibrium, kinetic, and thermodynamic. *Environ. Earth Sci.* **2019**, *78*, 106.
(42) Ayawei, N.; Ebelegi, A. N.; Wankasi, D. Modelling and interpretation of adsorption isotherms. *J. Chem.* **2017**, *2017*, No. 3039817.

https://doi.org/10.1021/acsomega.3c01609
ACS Omega 2023, 8, 17209−17219